

Research



Cite this article: Finet C, Ruan Q, Bei YY, You En Chan J, Saranathan V, Yang JKW, Monteiro A. 2023 Multi-scale dissection of wing transparency in the clearwing butterfly *Phanus vitreus*. *J. R. Soc. Interface* **20**: 20230135. <https://doi.org/10.1098/rsif.2023.0135>

Received: 9 March 2023

Accepted: 9 May 2023

Subject Category:

Life Sciences—Physics interface

Subject Areas:

biomaterials, biomimetics, biophysics

Keywords:

transparency, clearwing butterfly, hydrophobicity, structural coloration, HesperIIDae

Authors for correspondence:

Cédric Finet

e-mail: cedric.finet@ens-lyon.org

Joel K. W. Yang

e-mail: joel_yang@sutd.edu.sg

Antónia Monteiro

e-mail: antonia.monteiro@nus.edu.sg

[†]These authors contributed equally to this study.

[‡]Present address: Division of Sciences, School of Interwoven Arts and Sciences, Krea University, Sricity, India.

Electronic supplementary material is available online at <https://doi.org/10.6084/m9.figshare.c.6662179>.

Multi-scale dissection of wing transparency in the clearwing butterfly *Phanus vitreus*

Cédric Finet^{1,†}, Qifeng Ruan^{2,3,†}, Yi Yang Bei¹, John You En Chan², Vinodkumar Saranathan^{1,4,5,‡}, Joel K. W. Yang^{2,6} and Antónia Monteiro¹

¹Biological Sciences, National University of Singapore, 117543 Singapore

²Engineering Product Development, Singapore University of Technology and Design, 487372 Singapore

³Ministry of Industry and Information Technology Key Lab of Micro-Nano Optoelectronic Information System & Guangdong Provincial Key Laboratory of Semiconductor Optoelectronic Materials and Intelligent Photonic Systems, Harbin Institute of Technology, Shenzhen 518055, People's Republic of China

⁴Division of Science, Yale-NUS College, National University of Singapore, 138609 Singapore

⁵NUS Nanoscience and Nanotechnology Initiative (NUSNNI), National University of Singapore, 117581 Singapore

⁶Institute of Materials Research and Engineering, A*STAR (Agency for Science, Technology and Research), 138634 Singapore

✉ CF, 0000-0003-4196-9064; QR, 0000-0002-1592-9010; VS, 0000-0003-4058-5093; JKWY, 0000-0003-3301-1040; AM, 0000-0001-9696-459X

Optical transparency is rare in terrestrial organisms, and often originates through loss of pigmentation and reduction in scattering. The coloured wings of some butterflies and moths have repeatedly evolved transparency, offering examples of how they function optically and biologically. Because pigments are primarily localized in the scales that cover a colourless wing membrane, transparency has often evolved through the complete loss of scales or radical modification of their shape. Whereas bristle-like scales have been well documented in glasswing butterflies, other scale modifications resulting in transparency remain understudied. The butterfly *Phanus vitreus* achieves transparency while retaining its scales and exhibiting blue/cyan transparent zones. Here, we investigate the mechanism of wing transparency in *P. vitreus* by light microscopy, focused ion beam milling, microspectrophotometry and optical modelling. We show that transparency is achieved via loss of pigments and vertical orientation in normal paddle-like scales. These alterations are combined with an anti-reflective nipple array on portions of the wing membrane being more exposed to light. The blueish coloration of the *P. vitreus* transparent regions is due to the properties of the wing membrane, and local scale nanostructures. We show that scale retention in the transparent patches might be explained by these perpendicular scales having hydrophobic properties.

1. Introduction

Animal transparency, i.e. the physical state of letting light propagate through the body, is, arguably, the ultimate mechanism of camouflage [1]. Nearly transparent bodies are widespread in pelagic organisms such as jellyfish, sea angels, squids and fish [2,3]. Animal transparency is rare on land, yet we can cite a few instances in insects: the wings of most insects as well as those of glasswing butterflies [4], the prothorax and elytra margins of tortoise beetles [5] and the pupal case in many butterfly species just before eclosion [6]. In addition, cases of translucency have been described in amphibians, such as the glass frogs, the Barton Springs salamander and some tadpoles [7]. Translucency, which results in only partial transparency as a result of scattering from heterogeneous materials and interfaces [8], acts as modifiable camouflage by decreasing edge diffusion [9].

The wings of butterflies and moths (Lepidoptera) are a good model to study the development, the ecological function(s) and the evolution of transparency

from a non-transparent ancestral state. Wing transparency evolved several times independently during the diversification of Lepidoptera from ancestors with opaque wings [4]. Lepidopteran wings are typically covered with chitinous scales that bear colour produced by pigments [10,11], photonic nanostructures [12] or a combination of both [13–15]. Beyond their role in coloration, wing scales also play a role in thermoregulation [16,17] and water repellence [18]. As such, making wings transparent involves changing the development of scales, and potentially also their biological role.

Wing transparency can be achieved by a greater exposure of the wing membrane in different ways. Lepidoptera can simply lose scales [19–22], replace the typical flat, paddle-shaped scales by thin, hair-like piliform scales [18,23,24] or reduce pigmentation in the exposed membrane [4]. The replacement of archetypal, flattened scales with piliform ones has been thoroughly investigated in the glasswing butterfly *Greta oto*, which also uses surface waxes in the exposed membrane to reduce glare [25]. However, little is known about other potential ways of achieving transparency.

In the present study, we explore the structural basis and the function of the wing transparency in the musical ghost-skipper, *Phanus vitreus*, a clearwing butterfly in the family HesperIIDae, primarily found in lowland rainforests from Mexico to southern Brazil [26]. This species is remarkable for having evolved transparent wing patches while retaining scales in these patches [4], and exhibiting a unique visual effect due to the blue/cyan coloration of the transparent zones. The retention of scales suggests that they may have an important functional role. We applied optical and scanning electron microscopy (SEM), as well as focused ion beam (FIB) milling to characterize the structure of both the wing membrane and the wing scales in the transparent area. By combining UV–visible–near-infrared microspectrophotometry and optical modelling, we found that the transparent wing regions reflect blue and cyan light, and we disentangled the relative contribution of the wing membrane, the scales and the scale nanostructures to the overall coloration of the wing. Furthermore, contact angle goniometry showed that the modified scales of the transparent wing regions play a role in water repellence.

2. Results

2.1. Characterization of the transparent regions of the *Phanus vitreus* wing

The *P. vitreus* wing pigmentation pattern consists of a black background covered with pigmented scales, and several transparent ‘windows’ on both the forewing and the hindwing (figure 1*a,b*). The windows are not perfectly transparent, but rather show a light blue-green reflection (figure 1*a*), and a slight brownish tint when placed against a white background (figure 1*b*). The mean light transmittance is 85% in the visible regime under normal incidence (electronic supplementary material, figure S1). The transparent areas contain only one type of sparse scales, very short in length (approx. 40 μm ; figure 1*c*), and different from the flanking cover and ground black scales. These short scales have fused upper and lower laminae that are reminiscent of the fused scales of primitive Lepidoptera [27–29]. Contrary to the majority of butterfly scales, the scales of the transparent areas in *P. vitreus* do not

lie flat on the wing, but are attached almost perpendicular to the wing surface (average insertion angle of $80 \pm 5^\circ$) (figure 1*c,d*). When mounted on a black background and epi-illuminated, the wing membrane of the windows appears blue (figure 1*e*). When mounted on a glass slide and trans-illuminated, the same wing membrane shows an overall cyan hue (figure 1*f*). These observations prompted us to also investigate the basis of this blue–cyan coloration, in addition to the mechanisms of overall transparency.

2.2. Wing membrane of the windows: ultrastructure

To examine the mechanism of wing transparency, we first characterized the inner structure of the wing membrane by electron microscopy. SEM cross-sections of a torn wing showed that the wing membrane can be divided into three main cuticular layers: a dorsal and ventral exocuticle, and a mesocuticle as the middle layer (figure 2*a*). The exocuticle consists of a nipple array nanostructure (figure 2*b*), without wax, overlaying a lamellar organization (figure 2*c*). The nipple array has an average height of $h_n = 142 \pm 10$ nm and an average diameter of $d_n = 135 \pm 11$ nm (figure 2*a*). The nipple array is randomly arranged with an average pitch of 300 nm (figure 2*b*; electronic supplementary material, figure S2). SEM images did not show the presence of wax-based nanopillars on top of the nipple nanostructures described in the glasswing butterfly [25]. Nevertheless, we tested for any contribution of epicuticular wax to the wing membrane reflectance. We manually removed the scales by softly brushing a transparent wing region with a paintbrush (electronic supplementary material, figure S3), followed by plasma cleaning to remove surface hydrocarbons (electronic supplementary material, figure S4) [30]. Then, we measured the reflectance of the treated wing membrane. No significant difference was detected between the treated and untreated samples, suggesting that epicuticular wax does not play a role in the optical properties of the wing membrane in *P. vitreus* (electronic supplementary material, figure S5). Under the nipple array, the alternation of bright and dark layers, which is also visible in unstained samples (electronic supplementary material, figure S6*A*), likely results from a patterned distribution of pigment. The inner mesocuticle is made of a less dense material deposited perpendicular to the exocuticle (figure 2*a*). In the centre of this mesocuticle lies an electron-dense layer (visible in TEM) (figure 2*c*), whose persistence in unstained samples suggests its pigmented nature (electronic supplementary material, figure S6*A*).

The pigments present in the wing membrane, and which explain its pale brownish coloration (figure 1*b*), are likely melanins. This was confirmed by immersing wings in warm 3% H_2O_2 overnight, which breaks down melanin [31,32]. After H_2O_2 treatment, the wing membrane was less pigmented and exhibited a reduced visible-light absorbance (electronic supplementary material, figures S6*B* and S6*C*).

2.3. Wing membrane of the windows: photonics

In order to investigate how the nipples and the overall membrane structure impacted wing transparency, we used a modelling approach. Our model consists of a two-dimensional nipple array-based chitinous exocuticle with dimensions obtained from our TEM images (figure 2*d*). The nipple nanostructures were modelled as half ellipsoids with an average height of $h_n = 142 \pm 10$ nm, an average diameter of each

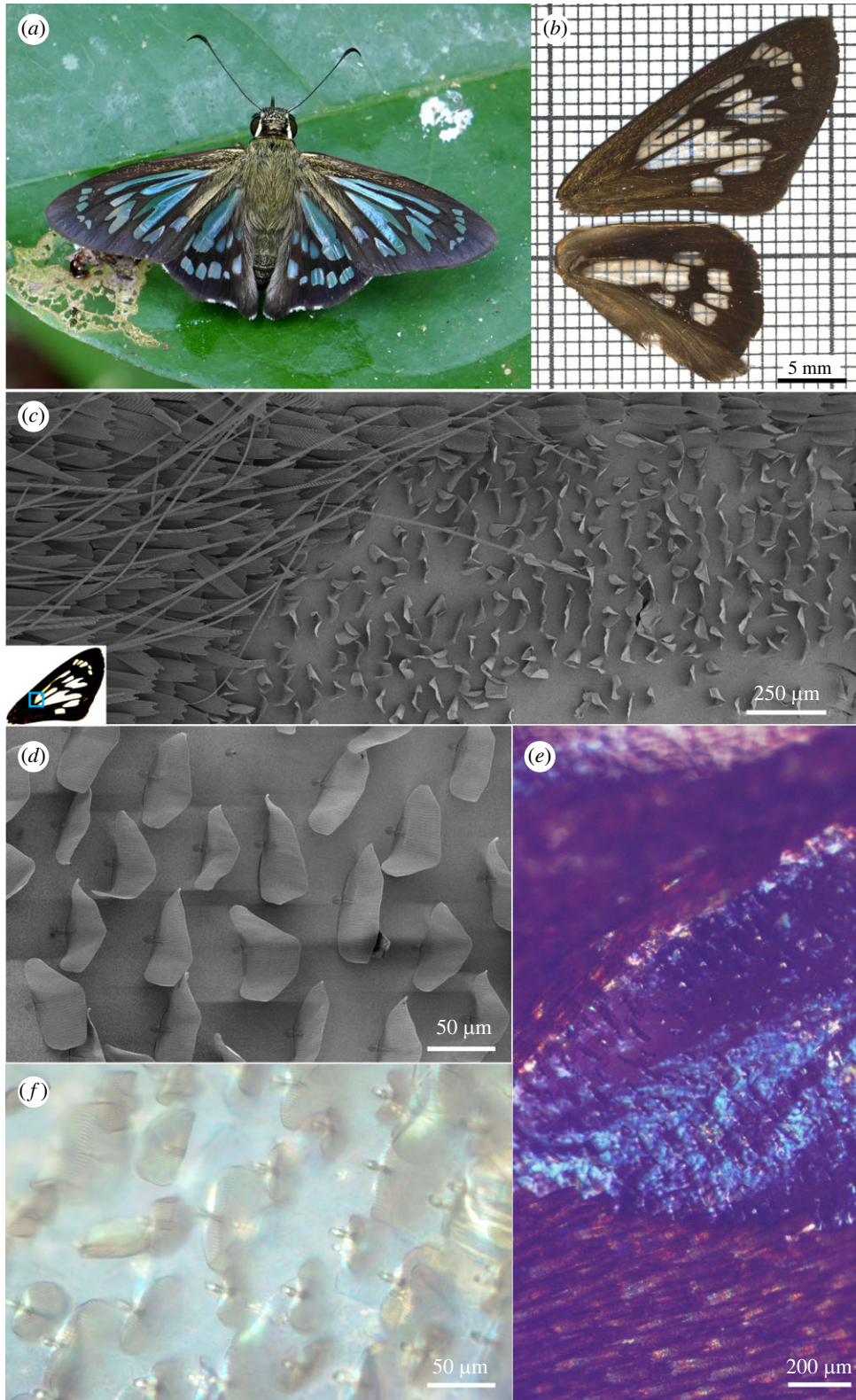


Figure 1. Multi-scale characterization of the clearwing musical ghost-skipper *Phanus vitreus*. (a) Adult *P. vitreus* beside Lake Soledad, Madre de Dios, Peru (photo: courtesy of Les Catchick). (b) Right fore- and hindwings mounted on graph paper. The grid is visible through the transparent windows of the *P. vitreus* wing. The transparent regions display a light brownish coloration. (c) SEM image of the edge between dark (left) and transparent (right) wing regions. The dark region is densely covered with flat, long and pigmented scales, whereas the transparent region shows sparse, small and nearly vertically arranged scales. Inset: the blue square highlights the wing area observed by SEM. (d) SEM close-up of the scales from the windows. (e) Epi-illumination of a transparent wing region mounted on carbon tape. (f) Transparent wing region mounted on a glass slide and examined with transmitted light.

nipple determined as $d_n = 135 \pm 11$ nm, and an average pitch (distance between two nipples) of 300 nm. We modelled the dorsal exocuticle with an average thickness of $h_{de} = 436 \pm 20$ nm, the pigmented mesocuticle with an average thickness of $h_m = 194 \pm 7$ nm and the ventral exocuticle with an average

thickness of $h_{ve} = 412 \pm 10$ nm, as per our direct measurements. Assuming that cuticle is mainly made of chitin, our optical model uses the refractive index of chitin $n = 1.56$ for both the dorsal and ventral exocuticles [33,34]. Estimating the refractive index of the pigmented mesocuticle required to consider the

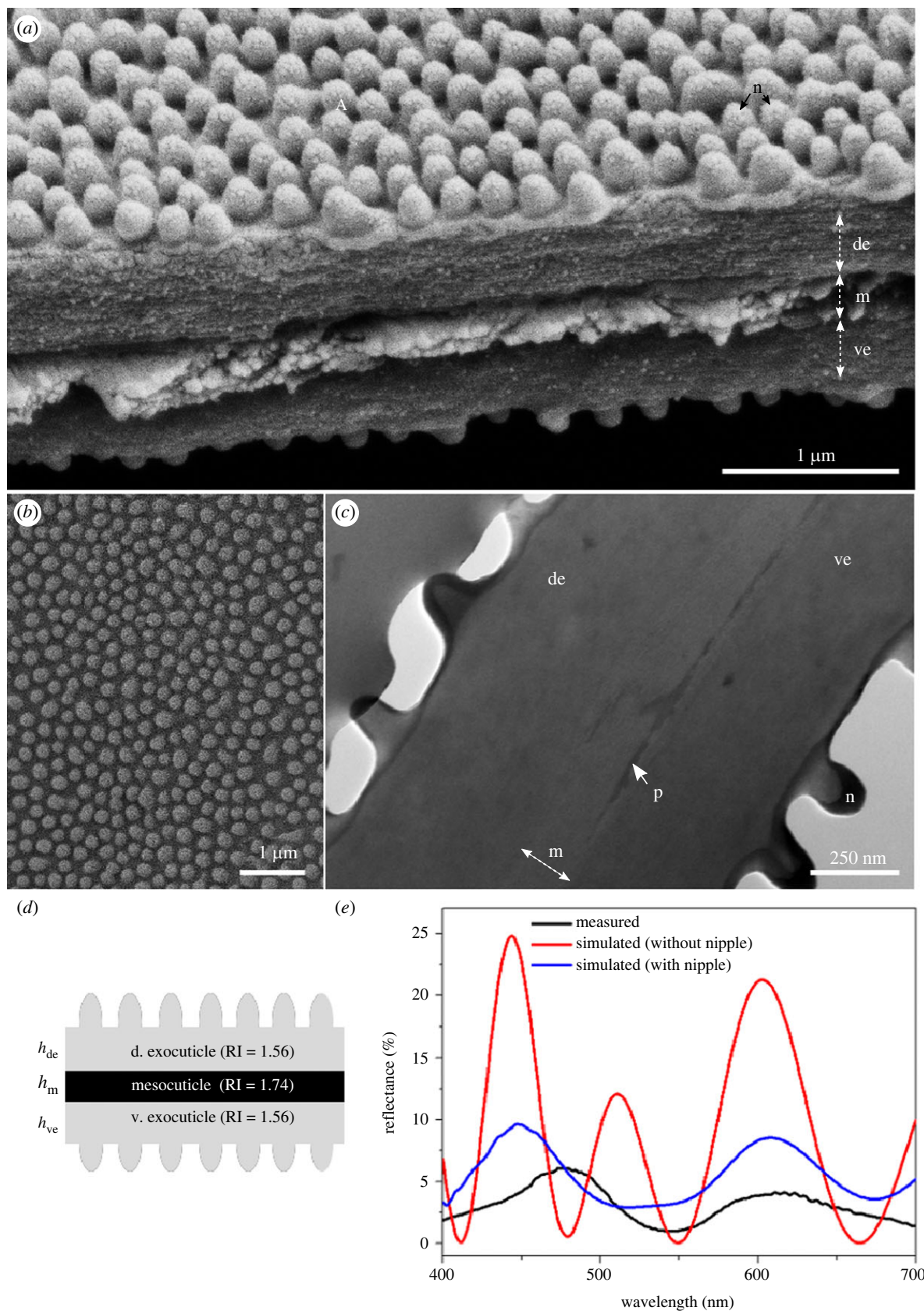


Figure 2. Structure and optical properties of the *Phanus vitreus* window wing membrane. (a) SEM close-up of a naturally torn transparent region of the wing. Two main cuticular layers are visible: the exocuticle and the mesocuticle. (b) SEM close-up of the wing membrane surface showing the regular arrangement of nipple array nanostructures. (c) TEM cross-section of the same sample without staining. (d) Best-fit optical model. (e) Measured and simulated reflectance. de, dorsal exocuticle; m, mesocuticle; n, nipple nanostructure; p, pigment; ve, ventral exocuticle.

effect of absorbing pigments. Light propagation in absorbing materials can be described using a complex-valued refractive index. The imaginary part explains the attenuation, while the real part accounts for refraction. We estimated the

wavelength-dependent imaginary part of the refractive index from our measured absorption spectrum as previously described [35]. The imaginary part is quite small (less than 0.012 in the visible range; electronic supplementary material,

figure S7), which makes the transparent wing possible. The real part of the refractive index of the pigment layer is 1.74, similar to previously reported values [36].

We then ran alternative models that differed in the inner structure of the wing membrane to examine which aspects of the membrane morphology altered light reflectance (hence transparency), and to pick the best-fitting model. The 'one-layer' model assumed a homogeneous cuticular content of the wing membrane, and led to a reflectance spectrum with multiple peaks that differed from the bimodal spectrum obtained experimentally (electronic supplementary material, figure S8A). The 'three-layer' model assumed the presence of melanin in the mesocuticle and considered the wing membrane as being slightly asymmetrical, with dorsal exocuticle thicker than ventral exocuticle. The simulated reflectance data using this model provided a better fit to the experimental reflectance data (figure 2e). A model where the ventral and dorsal exocuticle had the same thickness produced very similar results (electronic supplementary material, figure S8B), showing that the slight asymmetry of the membrane does not play a crucial role in its reflection. Comparing the previous 'three-layer' model *in silico* with a model in which the nipple nanostructures were absent, we obtained very similar spectral reflectance signatures, such as the position and shape of the peaks, but the reflectance intensity was significantly lower in the nipple model (figure 2e). This demonstrates that the nipple nanostructures decrease the reflectivity of the wing membrane, making the wing more transparent. The discrepancy between the simulated reflectance spectrum of the model with nipples and the measured reflectance spectrum could be ascribed to the non-uniformity of the cuticular thickness and nipple shape in the real wing membrane. Moreover, we plotted the simulated transmittance spectrum of the model with nipples (electronic supplementary material, figure S9). The transmittance value in the visible range is larger than 80%, which is consistent with the transparent appearance of the wing. We also simulated the electric field distributions for the 'three-layer' model with nipples (electronic supplementary material, figure S10). The electric field magnitudes above the light source at the peak/dip wavelengths of 440 nm, 543 nm and 607 nm are 0.34, 0.22 and 0.36, respectively.

2.4. Modified scales of the windows produce structural colour

We next looked at how the retention of scales on the wing membrane impacted wing membrane reflectance. We measured the spectral reflectance of both the intact transparent wing area and the same region after the removal of the scales. Reflectances were similar, but the intensity of the second peak (approx. 600 nm) was slightly reduced when the scales were removed (electronic supplementary material, figure S11). Thus, scales contribute to the overall reflectivity of the wing in *P. vitreus*, but their contribution at normal incidence is limited given their nearly upright orientation.

To investigate the contribution of the different hierarchical nanostructures of the scale to overall wing reflectivity, we examined the scales with SEM, FIB-SEM and optical imaging. The abwing (upperside) surface of the scale consists of a grid of longitudinal chitinous ridges (figure 3a), whereas the adwing (underside) surface is largely featureless (figure 3b). Under epi-illumination, the abwing surface displays a

predominant cyan hue with local yellow and orange tints (figure 3c). At higher magnification, the ridges show blue dots regularly spaced along their length (figure 3c'). The adwing surface appears bluer, with a Pointillist multi-coloured effect being visible at higher magnification (figure 3d'; electronic supplementary material, figure S12). Taken together, our observations suggest that the predominant cyan hue of the scale comes from the interridge region of the scale, and the deeper blue coloration comes from the ridge.

To test these hypotheses further, we measured the reflectance of each region of the scale with a microspectrophotometer. Whereas the reflectance spectrum of the interridge region shows a single peak around 520 nm, the reflectance spectrum of the ridge region comprises two peaks: centred around 410 and 520 nm (figure 3e). Because the minimum sample area of the microspectrophotometer ($1\ \mu\text{m} \times 1\ \mu\text{m}$) exceeds the width of the ridge (approx. 250 nm) and given the high numerical aperture of the objective (0.9), it is likely that the ridge measurement collected the light reflected from both the ridge and the surrounding interridge regions.

To further ascertain the effect of the ridge and interridge regions on scale colour production, we selectively removed a part of the ridge by FIB-SEM on an uncoated scale, then remeasured the reflectance of the milled ridge area. The first peak (approx. 410 nm) disappeared, whereas the second peak (approx. 520 nm) remained (figure 3e), suggesting that the ridge and the interridge region, respectively, give rise to the first and second peaks.

To further validate the structural basis of the scale coloration, we ran optical simulations. First, we built a simple optical model of the interridge region that consists of microribs (average thickness $h_{\text{mr}} = 45 \pm 2$ nm, average width $w_{\text{mr}} = 62 \pm 4$ nm, average distance between two microribs $d = 58 \pm 3$ nm) on top of a lower lamina (average thickness $h_{\text{LL}} = 225 \pm 12$ nm) (figure 3g). The resulting simulated reflectance shows a single peak around 520 nm, whose width is bigger (i.e. colour less saturated) than the one obtained for experimental measurements. We also investigated the impact of the distance between microribs on the reflectance by varying the microrib spacing in our model. We found that the reflection spectrum was blue-shifted towards shorter wavelengths when the distance between microribs was increased (electronic supplementary material, figure S13).

We then built an optical model of the ridge itself. The ridge consists of partly overlapping lamellae whose tip stands over an air layer (figure 3f). Under epi-illumination, the lamella tips exhibit a blue coloration, leading to the dotted appearance of the ridge (figure 3c'). We found that a multi-film interference model made of alternating materials with different refractive indices ($n_{\text{air}} = 1$, $n_{\text{chitin}} = 1.56$), recapitulates the empirical reflectance data. In our model, the top chitinous layer (the lamella) is separated from the bottom chitinous layer (the lower lamina of the scale) by a distance that corresponds to the average thickness of the air layer, h_{air} . The simulated reflectance shows a peak around 410 nm (figure 3g) that recapitulates the reflection measured for the ridge area (figure 3e).

2.5. Modified scales contribute to the hydrophobicity of the windows

The inclusion of these vertical-oriented scales increases the overall reflectivity of the wing membrane, making it less

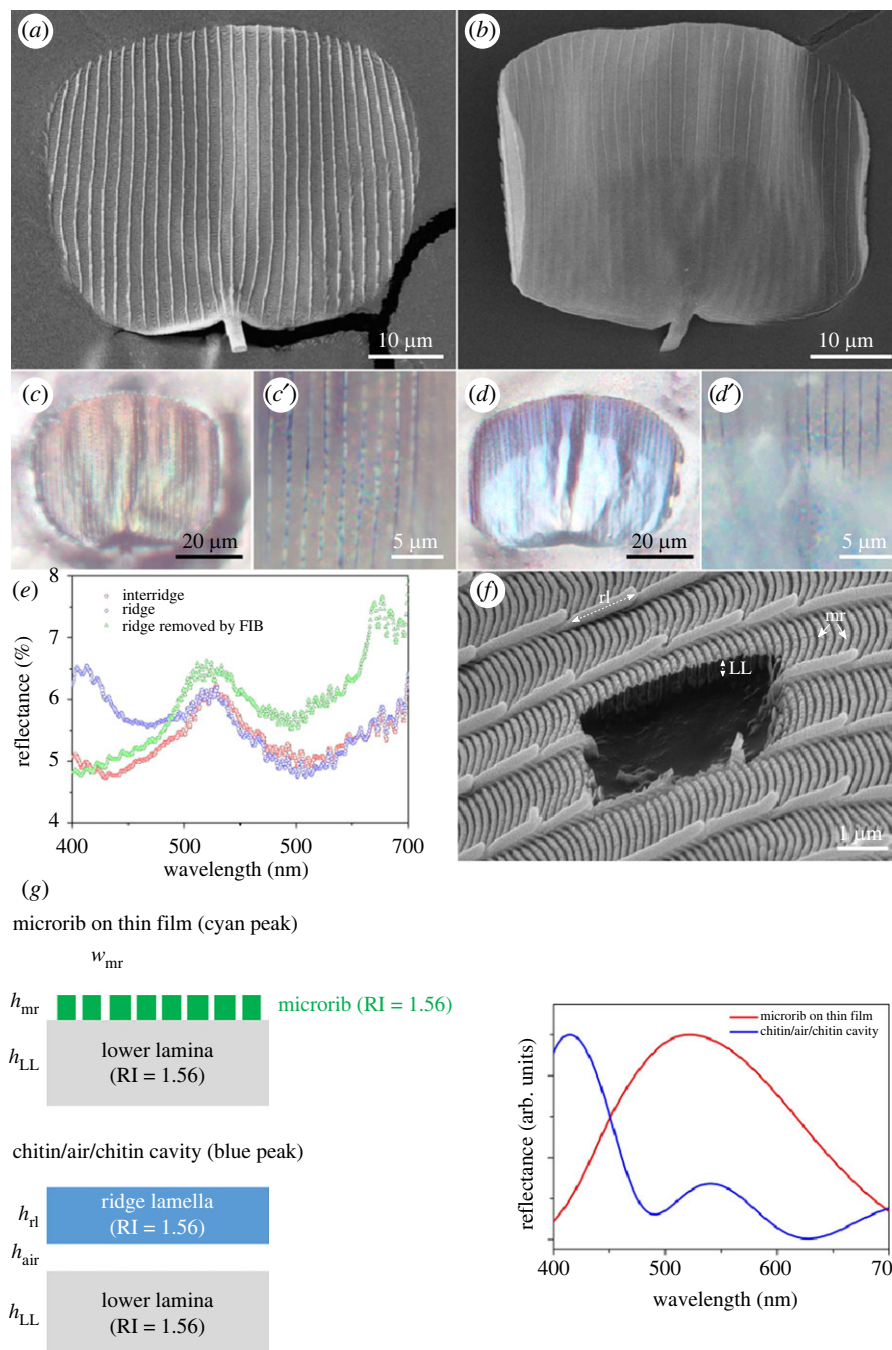


Figure 3. Structure and optical properties of the *Phanus vitreus* window scales. (a) SEM image of the abwing (upperside) surface and (b) SEM of the adwing (underside) surface of a scale. (c) Optical microscopy image of the abwing surface under epi-illumination using a 20 \times objective. (c') The same scale under a 100 \times objective. (d) Optical microscopy image of the adwing surface under epi-illumination using a 20 \times objective. (d') Same scale under a 100 \times objective. (e) Reflectance measured on different areas of the scale: the ridge (in blue), the ridge after its milling (in green), and the domain covered with microribs between two consecutive ridges, or the interridge (in red). (f) FIB-SEM cross-section of the scale. (g) Best-fitting optical models for the ridge and inter-ridge colorations, and resulting simulated reflectance. LL, lower lamina; mr, microrib; rl, ridge lamella.

transparent, so it is unclear why scales are retained at all in the transparent patches. In order to understand their putative biological function, we investigated the contribution of the vertical scales to the overall hydrophobicity of the transparent wing area. To do so, we placed a droplet of water on the wing surface and measured the contact angle of the droplet with the wing surface (figure 4a). The capability of a substrate to repel water (i.e. hydrophobicity) increases with increasing contact angles. A substrate is termed hydrophobic when the contact angle exceeds 90 $^\circ$, and superhydrophobic for values greater than 150 $^\circ$ [37]. We first assessed the hydrophobicity of the wing area

covered with normal black scales and found an average static contact angle ($^\circ$) of 145 \pm 3.2, which is highly hydrophobic (figure 4b) and comparable to values reported in other species [24]. Then we did the same calculations for the transparent region and found a significantly smaller average static contact angle of 114 \pm 6.9 (*t*-test, d.f. = 4, *p*-value = 1.8 \times 10 $^{-5}$). This value, however, is significantly more hydrophobic than the value of the membrane after manually removing the scales: 93 \pm 11.1 (*t*-test, d.f. = 4, *p*-value < 6.7 \times 10 $^{-3}$) (figure 4b). We conclude that retaining scales in the transparent area improves overall wing hydrophobicity.

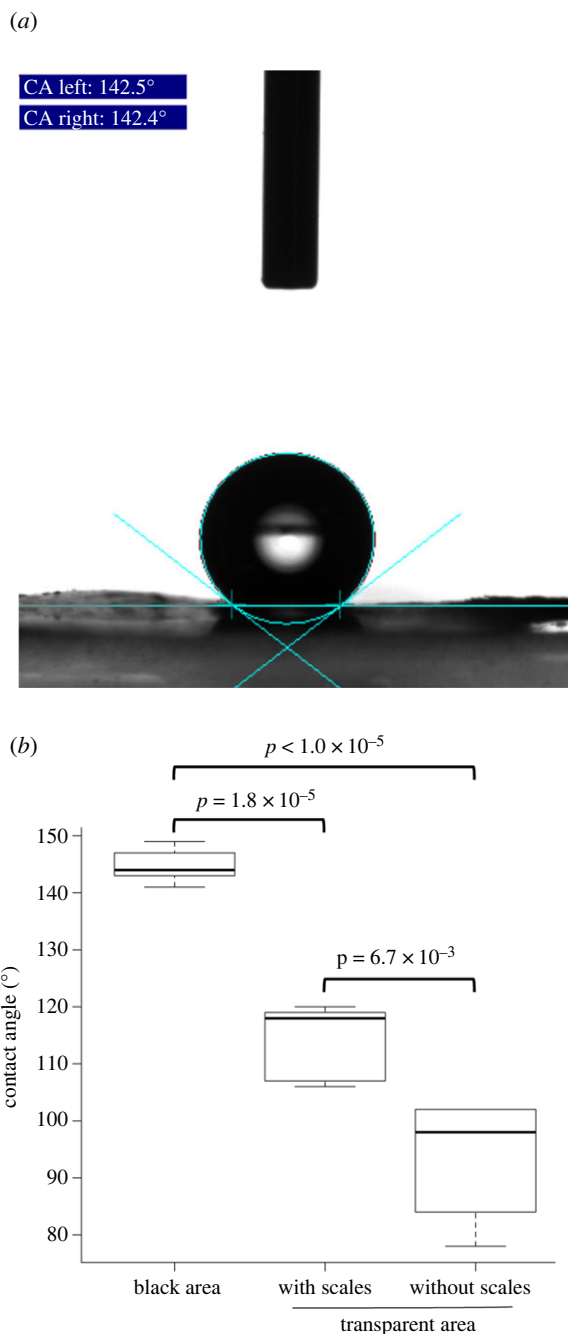


Figure 4. Contact angles on different areas of the *Phanus vitreus* wing. (a) Experimental set-up: a droplet of water is deposited on the wing by a capillary (visible on the image), then the baseline is manually defined and the geometry and angles of the droplet are extracted by the software. The present case shows an example where the left contact angle is 142.5° and the right angle is 142.4°. (b) Maximal contact angle is obtained for dark regions of the wing ($\theta_{\text{mean}} = 144.8^\circ$) that are therefore nearly superhydrophobic. Transparent regions of the wing are less hydrophobic than dark regions ($\theta_{\text{mean}} = 114^\circ$), and become significantly less hydrophobic when devoid of scales ($\theta_{\text{mean}} = 92.8^\circ$).

3. Discussion

3.1. Evolving sub-optimal wing transparency

Wing transparency has evolved multiple times independently across Lepidoptera [4], suggesting the ecological relevance of this trait. In Lepidoptera, transparency might play a role in thermoregulation as evidenced by the decreasing transmittance of the transparent wing area as latitude

increases in a large sample of species [4]. Transparency also serves as camouflage by allowing the resting background colours to emerge through the wings of diurnal butterflies [4,38,39] and nocturnal resting moths [40]. Furthermore, transparency has been shown to act as an aposematic signal among co-mimetic species [41].

Although the ecological relevance of wing transparency remains unknown in *P. vitreus* butterflies, the multiple mechanisms deployed to optimize this trait suggest important selective pressures on the evolution of transparency in this species and perhaps other lepidopterans. The nearly vertical orientation of the fairly short scales maximizes the exposure of the wing membrane to light. However, the wing membrane can still reflect light due to the stark difference in refractive index between air ($n = 1$) and chitin ($n = 1.56$) [42]. Light reflectance is reduced, however, via the nipple array on the surface of the wing membrane, which increases light transmission through the tissue. This strategy, as well as the deployment of wax nanopillars and conical protuberances to reduce light reflectance, have previously been observed in the wings of other species of butterflies [25,41,43–45], in the wings of moths [20,46], in the wings of cicadas [47,48] and in the eyes of moths [49,50] and other insects [51–53]. These natural strategies have also inspired the development of anti-reflective coatings [54–57].

Our findings, however, show that the windows on the *P. vitreus* wing deviate from perfect transparency. The light is not entirely transmitted through the wing, but partly absorbed by the pigment in the wing membrane and partly reflected by the encountered scale nanostructures. Interestingly, published studies of the glasswing butterfly *G. oto* do not mention the presence of pigment in the wing membrane, nor optical models that necessitate a pigmented wing membrane to fit the measured reflectance [25,43]. Future studies might help to determine whether the pigmentation of the *P. vitreus* wing membrane is a secondarily acquired trait, or alternatively, an ancestral feature in Lepidoptera that has been lost in other transparent species like *G. oto*. Another difference between these two species is that *P. vitreus*, in contrast to *G. oto*, shows no wax-based nanopillars on top of the nipple nanostructures. It has been shown that these wax-based nanopillars, mainly composed of long-chain *n*-alkanes, reinforce the anti-reflective properties of the nipples in *G. oto* [25] and in other butterflies [41]. Despite this difference in nanopillar composition, the transparent wings have a similar transmittance under normal incidence in *P. vitreus* (85%) and in *G. oto* (84%) [43].

3.2. Retaining scales in the transparent wing windows

The strategy ‘zero scales’ has evolved several times independently during the evolution of clearwing moths and butterflies [4]. This strategy, which seems rather ultimate and optimal, is however not the rule among clearwing lepidopterans with the majority of species retaining scales in the transparent wing regions [4]. A proximal explanation for such diversity is that different molecular mechanisms are responsible for the modification of the scales among clearwing lepidopterans. Whereas altered neural precursor formation would presumably lead to the absence of scales [58], as is the case for absence and variation in the location of homologous sensory bristles across insects [59–63], the perturbation of more downstream developmental genes

would affect the morphology and orientation of the scales [15,64]. An ultimate, adaptive hypothesis would be that retaining scales in transparent wing regions aids in generating structural colours [12], self-cleaning [65], aerodynamics [66] and thermoregulation [67]. Here, we demonstrate that the upright scales of the transparent regions in *P. vitreus* confer increased hydrophobicity to the wing, a function that might be generalized to most clearwing butterflies and moths [68].

3.3. Wing membrane and scales are coloured via thin-film interference

The transparent windows of *P. vitreus* have a lightly iridescent, blue–cyan coloration because the blue–cyan light is mainly reflected by the encountered nanostructures. We have shown that multi-layered thin-film interference explains the coloration both of the wing membrane and of the scale. Our findings show that the wing scales are able to produce structural colours when they stand horizontally under normal light incidence. Even if the nearly vertical and natural position of the scales partly annihilates this coloration, the scales still contribute to the overall coloration of the transparent windows in *P. vitreus*. Furthermore, it is noteworthy that *P. vitreus* belongs to the subfamily Pyrginae, whose representatives are known for basking with their wings held wide open, compared to the half-open wing basking position favoured by other hesperids, suggesting the putative ecological relevance of wing coloration in this species.

Alternatively, these blue hues might be used not for crypsis but for other biological functions. In the pipevine swallowtail butterfly, iridescent blue wing coloration is recognized as a warning signal by avian predators [69]. In *Morpho* butterflies, blue species have usually a fast and/or erratic flight that makes them difficult to locate and catch for birds. Blue in *Morpho* may serve as an escape aposematism by informing predators about the cost of an attack rather than toxicity [70,71]. Blue colours could also be used in mate recognition and choice in *Heliconius* butterflies [72]. Future ecological studies are required to understand the function of the blue–cyan colour in *P. vitreus*.

4. Material and methods

4.1. Biological samples

Dried specimens of *Phanus vitreus* were obtained from Lepidoptera Exchange (<https://lepidopexchange.com/>). The individuals were collected in San Vicente, Argentina in November 2007.

4.2. Optical imaging

Epi-illumination microscope images were obtained with either a 20× or 100× objective of a uSight-2000-Ni microspectrophotometer (Technospex Pte. Ltd, Singapore) and a Touptek U3CMOS-05 camera.

4.3. Scanning electron microscopy

Samples were mounted on carbon tape, and sputter-coated (JEOL JFC-1600) with platinum for 100 s at 40 mA. Samples were imaged using a FEI Versa 3D with the following parameters: voltage 10 kV, current 23 pA. Cross sections of wing scales were obtained by FIB milling using the gallium ion beam of the FEI Versa 3D with the following parameters: beam

voltage 8 kV, beam current 12 pA, tilt 52°. Milled samples were imaged as previously described. Thickness and other geometries were measured using the Line tool implemented in Fiji [73].

4.4. Transmission electron microscopy

Adult wings were fixed in 2.5% glutaraldehyde in phosphate-buffered saline (PBS, pH=7.4) for 4 h at 4°C. Wings were washed in PBS and post-fixed in 1% osmium tetroxide for 30 min. Samples were then dehydrated in ethanol and embedded in epoxy resin. Samples were sectioned on a Leica UCT ultramicrotome, stained with lead citrate and imaged with a JEOL JEM-1220 TEM at 100 kV. Thickness and other geometries were measured using the Line tool implemented in Fiji [73]. Ten independent measurements were taken and averaged.

4.5. Microspectrophotometry

Samples were mounted on carbon tape. Reflectance spectra with a usable range of 350–950 nm were acquired with a microspectrophotometry set-up using a mercury–xenon light source (Thorlabs, New Jersey, USA) connected to a uSight-2000-Ni microspectrophotometer (Technospex Pte. Ltd, Singapore), using a polished aluminium mirror as a light reference. The microscope's Nikon TU Plan Fluor objectives have the following specifications: 4× (NA = 0.13), 20× (NA = 0.5), 100× (NA = 0.9). Each measurement was averaged 10 times over an integration time of 100 ms. Reflectance spectra from three measurements taken at different locations on the same sample were averaged to account for any variability.

Transmittance spectra were measured using the same set-up, except that the samples were mounted on a glass slide. For reference, we used the light transmitted through the glass side. To obtain absorption spectra, the samples were mounted on a glass slide and covered with a coverslip, and immersed in clove oil as a refractive index matching medium for chitin. A transparent area of the glass substrate covered with clove oil was used as the reference. Transmittance and absorption spectra were obtained by averaging three measurements taken at different locations on the same sample.

4.6. Optical simulation

The electromagnetic simulations were conducted with a finite-difference time-domain software (Lumerical Solution Inc.). Chitin was modelled as a lossless material with a refractive index of 1.56. For the reflection spectra, a broadband plane wave was normally incident to the simulated membranes and scales. We used a periodic boundary condition in the x/y -direction and a perfectly matched layer-absorbing boundary condition in the z -direction to absorb light outside the structure regions. Energy monitors were placed behind the light source to record the calculated power flux and obtain the simulated reflection spectra. The electric field profiles in the plane of incidence at the peak/dip wavelengths were recorded by a field profile monitor.

4.7. Plasma cleaning

To remove surface hydrocarbons, we cut the wing into small pieces, manually removed the scales from the transparent region, and placed them in a plasma cleaner. Ultraviolet light generated in the plasma breaks most organic bonds of hydrocarbons [30]. Moreover, the radical oxygen species generated react with the broken-down organic contaminants to form mainly water and carbon dioxide that are continuously removed from the chamber. The samples were oxygen-plasma treated using a power of 60 W for durations of 20 and 120 s and a frequency of 13.56 MHz (PICO System, Diener Electronic, Ebhausen,

Germany). The oxygen flow rate was set at 15 standard cubic centimetres per minute (sccm). Reflectance was measured subsequently on three independent samples.

4.8. Contact angle measurement

In order to measure wing hydrophobicity, we calculated the static contact angle of small droplets of water placed on the surface of the wing. We performed five measurements on non-overlapping transparent regions of the dorsal forewings, on the same transparent region after we manually removed the scales, and on black wing regions. Measures were acquired with an OCA40 Micro system (DataPhysics Instruments GmbH, Filderstadt, Germany) at 25°C with a defined drop volume of 1 µl of ultra-pure water. A video was recorded after the drop was dispensed, and then we used SCA20 software (DataPhysics Instruments GmbH, Filderstadt, Germany) to calculate the static contact angle. Statistical analysis and boxplots were performed using R statistics package version 3.5.0 (the R Project for Statistical Computing, <https://www.r-project.org>).

Data accessibility. The raw data are available on Zenodo (<https://doi.org/10.5281/zenodo.7824043>) [74].

The data are provided in electronic supplementary material [75].

References

1. Bagge LE. 2019 Not as clear as it may appear: challenges associated with transparent camouflage in the ocean. *Integr. Comp. Biol.* **59**, 1653–1663. (doi:10.1093/icb/icz066)
2. Mcfall-Ngai MJ. 1990 Crypsis in the pelagic environment. *Integr. Comp. Biol.* **30**, 175–188. (doi:10.1093/icb/30.1.175)
3. Johnsen S. 2001 Hidden in plain sight: the ecology and physiology of organismal transparency. *Biol. Bull.* **201**, 301–318. (doi:10.2307/1543609)
4. Gomez D *et al.* 2021 Wing transparency in butterflies and moths: structural diversity, optical properties, and ecological relevance. *Ecol. Monogr.* **91**, e01475. (doi:10.1002/ecm.1475)
5. Pasteels JM, Deparis O, Mouchet SR, Windsor DM, Billen J. 2016 Structural and physical evidence for an endocuticular gold reflector in the tortoise beetle, *Charidotella ambita*. *Arthropod. Struct. Dev.* **45**, 509–518. (doi:10.1016/j.asd.2016.10.008)
6. Van Son G. 1955 Genus Danaus Kluk. *Transvaal Museum Mem.* **8**, 2–8.
7. Frost DR. 2011 *Amphibian species of the world: an online reference*. Version 5.5 (31 January 2011). Electronic Database. New York, NY: American Museum of Natural History.
8. Hecht E. 1987 *Optics*. Reading, MA: Addison-Wesley.
9. Barnett JB, Michalis C, Anderson HM, McEwen BL, Yeager J, Pruitt JN, Scott-Samuel NE, Cuthill IC. 2020 Imperfect transparency and camouflage in glass frogs. *Proc. Natl Acad. Sci. USA* **117**, 12 885–12 890. (doi:10.1073/pnas.1919471117)
10. Beldade P, Monteiro A. 2021 Eco-evo-devo advances with butterfly eyespots. *Curr. Opin. Genet. Dev.* **69**, 6–13. (doi:10.1016/j.gde.2020.12.011)
11. Van Belleghem SM, Lewis JJ, Rivera ES, Papa R. 2021 Heliconius butterflies: a window into the evolution and development of diversity. *Curr. Opin. Genet. Dev.* **69**, 72–81. (doi:10.1016/j.gde.2021.01.010)
12. Lloyd VJ, Nadeau NJ. 2021 The evolution of structural colour in butterflies. *Curr. Opin. Genet. Dev.* **69**, 28–34. (doi:10.1016/j.gde.2021.01.004)
13. Stavenga DG, Leertouwer HL, Wilts BD. 2014 Coloration principles of nymphaline butterflies—thin films, melanin, ommochromes and wing scale stacking. *J. Exp. Biol.* **217**, 2171–2180. (doi:10.1242/jeb.098673)
14. Thayer R, Allen F, Patel NH. 2020 Structural color in Junonia butterflies evolves by tuning scale lamina thickness. *Elife* **9**, e52187. (doi:10.7554/eLife.52187)
15. Prakash A, Finet C, Banerjee T Das, Saranathan V, Monteiro A. 2022 Antennapedia and optix regulate metallic silver wing scale development and cell shape in *Bicyclus anynana* butterflies. *Cell Rep.* **40**, 111052. (doi:10.1016/j.celrep.2022.111052)
16. Berthier S. 2005 Thermoregulation and spectral selectivity of the tropical butterfly *Prepona meander*: a remarkable example of temperature auto-regulation. *Appl. Phys. A Mater. Sci. Process.* **80**, 1397–1400. (doi:10.1007/s00339-004-3185-x)
17. Krishna A, Nie X, Warren AD, Llorente-Bousquets JE, Briscoe AD, Lee J. 2020 Infrared optical and thermal properties of microstructures in butterfly wings. *Proc. Natl Acad. Sci. USA* **117**, 1566–1572. (doi:10.1073/pnas.1906356117)
18. Wanasekara ND, Chalivendra VB. 2011 Role of surface roughness on wettability and coefficient of restitution in butterfly wings. *Soft Matter* **7**, 373–379. (doi:10.1039/c0sm00548g)
19. Yoshida A, Motoyama M, Kosaku A, Miyamoto K. 1996 Nanoprotuberance array in the transparent wing of a hawkmoth, *Cephonodes hylas*. *Zool. Sci.* **13**, 525–526. (doi:10.2108/zsj.13.525)
20. Yoshida A, Motoyama M, Kosaku A, Miyamoto K. 1997 Antireflective nanoprotuberance array in the transparent wing of a hawkmoth, *Cephonodes hylas*. *Zool. Sci.* **14**, 737–741. (doi:10.2108/zsj.14.737)
21. Farina JL. 2001 Aportes al conocimiento de la bionomía de Heliconisa pagenstechei (Lepidoptera: Saturniidae). *Rev. la Soc. Entomológica Argentina* **60**, 125–128.
22. Schmidt BC. 2018 Cryptic species among bumblebee mimics: an unrecognized *Hemaris* hawkmoth (Lepidoptera: Sphingidae) in eastern North America. *Zootaxa* **4399**, 32–48. (doi:10.11646/zootaxa.4399.1.2)
23. Hernández-Chavarría F, Hernández A, Sittenfeld A. 2004 The ‘windows’, scales, and bristles of the tropical moth *Rothschildia lebeau* (Lepidoptera: Saturniidae). *Rev. Biol. Trop.* **52**, 919–926.
24. Perez Goodwyn P, Maezono Y, Hosoda N, Fujisaki K. 2009 Waterproof and translucent wings at the same time: problems and solutions in butterflies. *Naturwissenschaften* **96**, 781–787. (doi:10.1007/s00114-009-0531-z)
25. Pomerantz AF, Siddique RH, Cash EI, Kishi Y, Pinna C, Hammar K, Gomez D, Elias M, Patel NH. 2021 Developmental, cellular and biochemical basis of transparency in clearwing butterflies. *J. Exp. Biol.* **224**, jeb237917. (doi:10.1242/jeb.237917)
26. Austin GT. 1993 A review of the *Phanus vitreus* group (Lepidoptera: Hesperidae: Pyrginae). *Trop. Lepid.* **4**, 21–36.

27. Kristensen NP. 1970 Morphological observations on the wing scales in some primitive Lepidoptera (Insecta). *J. Ultrastructure Res.* **30**, 402–410. (doi:10.1016/S0022-5320(70)80071-5)
28. Zhang Q *et al.* 2018 Fossil scales illuminate the early evolution of lepidopterans and structural colors. *Sci. Adv.* **4**, e1700988. (doi:10.1126/sciadv.1700988)
29. Kilchoer C, Steiner U, Wilts BD. 2019 Thin-film structural coloration from simple fused scales in moths. *Interface Focus* **9**, 20180044. (doi:10.1098/rsfs.2018.0044)
30. Ishibe Y, Kokai H, Oyama H, Sakamoto Y. 1988 Decarbonization by using ECR plasma. *Jpn. J. Appl. Phys.* **27**, 663. (doi:10.1143/JJAP.27.663)
31. Momose M, Ota H, Hayama M. 2011 Re-evaluation of melanin bleaching using warm diluted hydrogen peroxide for histopathological analysis. *Pathol. Int.* **61**, 345–350. (doi:10.1111/j.1440-1827.2011.02667.x)
32. Stavenga DG, Leertouwer HL, Hariyama T, De Raedt HA, Wilts BD. 2012 Sexual dichromatism of the damselfly *Calopteryx japonica* caused by a melanin-chitin multilayer in the male wing veins. *PLoS ONE* **7**, e49743. (doi:10.1371/journal.pone.0049743)
33. Leertouwer HL, Wilts BD, Stavenga DG. 2011 Refractive index and dispersion of butterfly chitin and bird keratin measured by polarizing interference microscopy. *Opt. Express* **19**, 24 061–24 066. (doi:10.1364/oe.19.024061)
34. Yoshioka S, Kinoshita S. 2011 Direct determination of the refractive index of natural multilayer systems. *Phys. Rev. E* **83**, 051917. (doi:10.1103/PhysRevE.83.051917)
35. Trzeciak TM, Wilts BD, Stavenga DG, Vukusic P. 2012 Variable multilayer reflection together with long-pass filtering pigment determines the wing coloration of papilionid butterflies of the nireus group. *Opt. Express* **20**, 8877–8890. (doi:10.1364/oe.20.008877)
36. Stavenga DG, Leertouwer HL, Wilts BD. 2013 Quantifying the refractive index dispersion of a pigmented biological tissue using Jamin-Lebedeff interference microscopy. *Light Sci. Appl.* **2**, e100. (doi:10.1038/lsa.2013.56)
37. Roach P, Shirtcliffe NJ, Newton MI. 2008 Progress in superhydrophobic surface development. *Soft Matter* **4**, 224–240. (doi:10.1039/b712575p)
38. Arias M, Mappes J, Desbois C, Gordon S, McClure M, Elias M, Nokelainen O, Gomez D. 2019 Transparency reduces predator detection in mimetic clearwing butterflies. *Funct. Ecol.* **33**, 1110–1119. (doi:10.1111/1365-2435.13315)
39. McClure M *et al.* 2019 Why has transparency evolved in aposematic butterflies? Insights from the largest radiation of aposematic butterflies, the Ithomiini. *Proc. R. Soc. B* **286**, 20182769. (doi:10.1098/rspb.2018.2769)
40. Arias M, Elias M, Andraud C, Berthier S, Gomez D. 2020 Transparency improves concealment in cryptically coloured moths. *J. Evol. Biol.* **33**, 247–252. (doi:10.1111/jeb.13560)
41. Pinna CS *et al.* 2021 Mimicry can drive convergence in structural and light transmission features of transparent wings in Lepidoptera. *Elife* **10**, e69080. (doi:10.7554/eLife.69080)
42. Vukusic P, Sambles JR, Lawrence CR, Wootton RJ. 1999 Quantified interference and diffraction in single Morpho butterfly scales. *Proc. R. Soc. Lond. B* **266**, 1403. (doi:10.1098/rspb.1999.0794)
43. Siddique RH, Gomard G, Hölscher H. 2015 The role of random nanostructures for the omnidirectional anti-reflection properties of the glasswing butterfly. *Nat. Commun.* **6**, 6909. (doi:10.1038/ncomms7909)
44. Binetti VR, Schiffman JD, Leaffer OD, Spanier JE, Schauer CL. 2009 The natural transparency and piezoelectric response of the *Greta oto* butterfly wing. *Integr. Biol.* **1**, 324–329. (doi:10.1039/b820205b)
45. Narasimhan V, Siddique RH, Lee JO, Kumar S, Ndjamen B, Du J, Hong N, Sretavan D, Choo H. 2018 Multifunctional biophotonic nanostructures inspired by the longtail glasswing butterfly for medical devices. *Nat. Nanotechnol.* **13**, 512–519. (doi:10.1038/s41565-018-0111-5)
46. Deparis O, Mouchet S, Dellieu L, Colomer JF, Sarrazin M. 2014 Nanostructured surfaces: bioinspiration for transparency, coloration and wettability. *Mater. Today: Proceedings* **1**, 122–129. (doi:10.1016/j.matpr.2014.09.008)
47. Watson GS, Watson JA. 2004 Natural nano-structures on insects: possible functions of ordered arrays characterized by atomic force microscopy. *Appl. Surf. Sci.* **235**, 139–144. (doi:10.1016/j.apsusc.2004.05.129)
48. Stoddart PR, Cadusch PJ, Boyce TM, Erasmus RM, Comins JD. 2006 Optical properties of chitin: surface-enhanced Raman scattering substrates based on antireflection structures on cicada wings. *Nanotechnology* **17**, 680–686. (doi:10.1088/0957-4484/17/3/011)
49. Bernhard CG, Miller WH, Moller AR. 1965 The insect corneal nipple array. *Acta Physiol. Scand.* **63**, 1–25. (doi:10.1111/j.1748-1716.1965.tb04037.x)
50. Clapham PB, Hutley MC. 1973 Reduction of lens reflexion by the 'Moth Eye' principle. *Nature* **244**, 281–282. (doi:10.1038/244281a0)
51. Bernhard CG, Gemme G, Sällström J. 1970 Comparative ultrastructure of corneal surface topography in insects with aspects on phylogenesis and function. *Z. Vgl. Physiol.* **67**, 1–25. (doi:10.1007/BF00298117)
52. Stavenga DG, Foletti S, Palasantzas G, Arikawa K. 2006 Light on the moth-eye corneal nipple array of butterflies. *Proc. R. Soc. B* **273**, 661–667. (doi:10.1098/rspb.2005.3369)
53. Kryuchkov M, Bilousov O, Lehmann J, Fiebig M, Katanaev VL. 2020 Reverse and forward engineering of *Drosophila* corneal nano-coatings. *Nature* **585**, 383–389. (doi:10.1038/s41586-020-2707-9)
54. Raut HK, Ganesh VA, Nair AS, Ramakrishna S. 2011 Anti-reflective coatings: a critical, in-depth review. *Energy Environ. Sci.* **4**, 3779–3804. (doi:10.1039/c1ee01297e)
55. Zada I, Zhang W, Li Y, Sun P, Cai N, Gu J, Liu Q, Su H, Zhang D. 2016 Angle dependent antireflection property of TiO₂ inspired by cicada wings. *Appl. Phys. Lett.* **109**, 153701. (doi:10.1063/1.4962903)
56. Kuo WK, Hsu JJ, Nien CK, Yu HH. 2016 Moth-eye-inspired biophotonic surfaces with antireflective and hydrophobic characteristics. *ACS Appl. Mater. Interfaces* **8**, 32 021–32 030. (doi:10.1021/acsami.6b10960)
57. Nien CK, Yu HH. 2019 The applications of biomimetic cicada-wing structure on the organic light-emitting diodes. *Mater. Chem. Phys.* **227**, 191–199. (doi:10.1016/j.matchemphys.2019.01.059)
58. Galant R, Skeath JB, Paddock S, Lewis DL, Carroll SB. 1998 Expression pattern of a butterfly achaete-scute homolog reveals the homology of butterfly wing scales and insect sensory bristles. *Curr. Biol.* **8**, 807–813. (doi:10.1016/S0960-9822(98)70322-7)
59. Campuzano S, Carramolino L, Cabrera CV, Ruiz-Gómez M, Villares R, Boronat A, Modolell J. 1985 Molecular genetics of the achaete-scute gene complex of *D. melanogaster*. *Cell* **40**, 327–338. (doi:10.1016/0092-8674(85)90147-3)
60. Hinz U, Giebel B, Campos-Ortega JA. 1994 The basic-helix-loop-helix domain of *Drosophila* lethal of scute protein is sufficient for proneural function and activates neurogenic genes. *Cell* **76**, 77–87. (doi:10.1016/0092-8674(94)90174-0)
61. Wheeler SR, Carrico ML, Wilson BA, Brown SJ, Skeath JB. 2003 The expression and function of the achaete-scute genes in *Tribolium castaneum* reveals conservation and variation in neural pattern formation and cell fate specification. *Development* **130**, 4373–4381. (doi:10.1242/dev.00646)
62. Finet C, Decaras A, Armisen D, Khila A. 2018 The achaete-scute complex contains a single gene that controls bristle development in the semi-aquatic bugs. *Proc. R. Soc. B* **285**, 20182387. (doi:10.1098/rspb.2018.2387)
63. Finet C, Decaras A, Rutkowska M, Roux P, Collaudin S, Juncour P, Viala S, Khila A. 2022 Leg length and bristle density, both necessary for water surface locomotion, are genetically correlated in water striders. *Proc. Natl Acad. Sci. USA* **119**, e2119210119. (doi:10.1073/pnas.2119210119)
64. Matsuoka Y, Monteiro A. 2018 Melanin pathway genes regulate color and morphology of butterfly wing scales. *Cell Rep.* **24**, 56–65. (doi:10.1016/j.celrep.2018.05.092)
65. Wagner T, Neinhuis C, Barthlott W. 1996 Wettability and contaminability of insect wings as a function of their surface sculptures. *Acta Zool.* **77**, 213–225. (doi:10.1111/j.1463-6395.1996.tb01265.x)
66. Slegers N, Heilman M, Cranford J, Lang A, Yoder J, Habegger ML. 2017 Beneficial aerodynamic effect of wing scales on the climbing flight of butterflies. *Bioinspir. Biomim.* **12**, 016013. (doi:10.1088/1748-3190/aa551d)
67. Tsai CC, Childers RA, Nan Shi N, Ren C, Pelaez JN, Bernard GD, Pierce NE, Yu N. 2020 Physical and behavioral adaptations to prevent overheating of the living wings of butterflies. *Nat. Commun.* **11**, 551. (doi:10.1038/s41467-020-14408-8)
68. Gomez D *et al.* 2021 Hydrophobicity in clearwing butterflies and moths: impact of scale micro and nanostructure, and trade-off with optical transparency. *bioRxiv*. (doi:10.1101/2021.10.11.463886)
69. Pegram KV, Lillo MJ, Rutowski RL. 2013 Iridescent blue and orange components contribute to the recognition of a multicomponent warning signal. *Behaviour* **150**, 321–336. (doi:10.1163/1568539x-00003053)

70. Pinheiro CEG, Freitas AVL, Campos VC, DeVries PJ, Penz CM. 2016 Both palatable and unpalatable butterflies use bright colors to signal difficulty of capture to predators. *Neotrop. Entomol.* **45**, 107–113. (doi:10.1007/s13744-015-0359-5)
71. Debat V, Berthier S, Blandin P, Chazot N, Elias M, Gomez D, Llaurens V. 2018 Why are *Morpho* blue? In *Biodiversity and evolution* (eds P Grandcolas, M-C Maurel), pp. 139–174. Oxford, UK: Elsevier. (doi:10.1016/B978-1-78548-277-9.50009-7)
72. Sweeney A, Jiggins C, Johnsen S. 2003 Insect communication: polarized light as a butterfly mating signal. *Nature* **423**, 31–32. (doi:10.1038/423031a)
73. Schindelin J *et al.* 2012 Fiji: an open-source platform for biological-image analysis. *Nat. Methods* **9**, 676–682. (doi:10.1038/nmeth.2019)
74. Finet C. 2023 Code for: *Phanus vitreus*—wing transparency optics [Data set]. *Zenodo*. (doi:10.5281/zenodo.7824043)
75. Finet C, Ruan Q, Bei YY, You En Chan J, Saranathan V, Yang JKW, Monteiro A. 2023 Multi-scale dissection of wing transparency in the clearwing butterfly *Phanus vitreus*. Figshare. (doi:10.6084/m9.figshare.c.6662179)